Electrochemical properties of bare nickel sulfide and nickel sulfide–carbon composites prepared by one-pot spray pyrolysis as anode materials for lithium secondary batteries
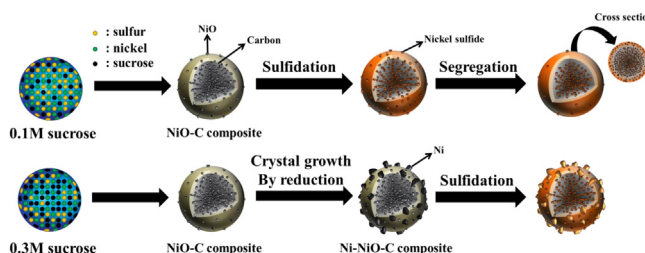
Mun Yeong Son, Jeong Hoo Choi, Yun Chan Kang*

Department of Chemical Engineering, Konkuk University, 1 Hwayang-dong, Gwangjin-gu, Seoul 143-701, Republic of Korea

HIGHLIGHTS

- Spherical bare nickel sulfide and nickel sulfide–carbon composite powders are prepared by a one-step spray pyrolysis.
- Nickel sulfide nanocrystals with a size of a few nanometers are uniformly distributed inside the spherical carbon matrix.
- Nickel sulfide–carbon composite powders have an excellent discharge capacity of 472 mA h g^{-1} even after 500 cycles.

GRAPHICAL ABSTRACT

ABSTRACT

Spherical bare nickel sulfide and nickel sulfide–carbon composite powders are prepared by a one-step spray pyrolysis. Submicron bare nickel sulfide particles with a dense structure have mixed crystal phases of NiS, Ni$_7$S$_6$, and Ni$_x$S$_6$. The nickel sulfide–carbon composite powders prepared from a spray solution containing 0.1 M sucrose have a main crystal structure of Ni$_7$S$_6$ phase with small impurity peaks of Ni$_x$S$_6$ phase. A nickel oxide–carbon composite powder is first formed as an intermediate product in the front part of the reactor at 800 °C. Fast decomposition of thiourea at this high temperature results in the evolution of hydrogen sulfide gas, which then forms the nickel sulfide–carbon composite powders by direct sulfidation of nickel oxide under the reducing atmosphere. Nickel sulfide nanocrystals with a size of a few nanometers are uniformly distributed inside the spherical carbon matrix. The nickel sulfide–carbon composite powders prepared with 0.1 M sucrose have an excellent discharge capacity of 472 mA h g^{-1} at a high current density of 1000 mA g^{-1}, even after 500 cycles, with the corresponding capacity retention measured after the first cycle being 86%.

© 2013 Elsevier B.V. All rights reserved.

1. Introduction

Metal sulfides have been attracting a great deal of attention from researchers owing to their distinct electrical and optical properties compared to those of the corresponding metal oxides [1]. A number of different compositions of metal sulfides have been considered for applications such as in batteries, catalysts, electrochromic devices, solar energy devices and so on [2–7]. In particular, nickel sulfides have been studied as potential active materials for lithium secondary batteries because of their high theoretical capacity characteristics [7–9]. However, one of the drawbacks of using nickel sulfides for such an application is that they exhibit poor electrochemical properties at high current densities. Various methods, such as applying dopants, coating layers, and forming

* Corresponding author. Tel.: +82 2 2049 6010; fax: +82 2 458 3504.
  E-mail address: yckang@konkuk.ac.kr (Y.C. Kang).

composites, have been evaluated for improving the rate performances of nickel sulfide anode materials. Iron-doped nickel disulfide has demonstrated good cycling characteristics, with the iron atoms stabilizing the crystal structure by replacing some of the nickel atoms and slowing down the reduction in capacity [10]. Takeuchi et al. achieved improvements in the electrochemical properties of nickel sulfide by applying a surface coating of titanium dioxide or zirconium dioxide [11], while Mahmood et al. prepared a composite with nitrogen-doped graphene [12]. Graphene is well known as a support material for use in applications such as this, owing to its superior electrical conductivity, flexible volume expansion, high surface-to-volume ratio, and chemical stability [8,13,14]. However, the preparation of spherical nickel sulfide—carbon composite powders with high density and their electrochemical properties have not been studied in detail.

Nickel sulfide-based materials prepared using solid-state reactions and solution methods have been commonly used to prepare the anode of lithium secondary batteries [12,15]. As an alternative approach, the gas-phase spray pyrolysis technique has a number of advantages for the preparation of spherical metal sulfide particles. Sulfide powders containing a single metal have been formed from a droplet containing a metal salt and sulfur source in a one-pot process. Various types of metal sulfides, including zinc, copper, cadmium, and molybdenum compounds, have been successfully produced using the spray pyrolysis process [16—20]. However, to the best of our knowledge, the electrochemical properties of metal sulfide powders prepared using this particular technique have not been reported thus far.

In this study, bare nickel sulfide and nickel sulfide—carbon composite powders were first prepared using a simple one-pot spray pyrolysis process. The carbon contents of the composite powders were controlled by changing the concentration of the sucrose carbon source dissolved in the spray solutions. The electrochemical properties of the resulting nickel sulfide—carbon composite powders were subsequently evaluated and compared to those of the bare nickel sulfide powders.

2. Experimental

Bare nickel sulfide and nickel sulfide—carbon composite powders were prepared by ultrasonic spray pyrolysis. A 1.7 MHz ultrasonic spray generator with six vibrators was used to generate a large amount of droplets. The inner diameter and length of the quartz reactor in the generator were 55 mm and 1.2 m, respectively. The reactor temperature was maintained at 800 °C, and the flow rate of the nitrogen used as the carrier gas was fixed at 5 L min^{-1}. The spray solution was prepared by dissolving nickel nitrate [$Ni(NO_3)_2 \cdot 6H_2O$, Junsei, Japan] and thiourea [HN_2NCSNH_2, Junsei] in distilled water. A thiourea quantity in excess of 100% of the stoichiometric amount necessary to form nickel sulfide was added to the spray solution. Sucrose was used as the carbon source for forming the nickel sulfide—carbon composites. The overall concentrations of nickel and sulfur components in the spray solution were 0.5 M, and the concentration of sucrose dissolved in the spray solution was varied from 0.03 to 0.3 M.

The crystal structures of the bare nickel sulfide and nickel sulfide—carbon composites were investigated using X-ray diffractometry (XRD, Rigaku DMAX-33) using Cu Kα radiation ($\lambda = 1.5418$ Å) at the Korea Basic Science Institute (Daegu). The morphologies of the precursor powders were characterized using scanning electron microscopy (SEM, JEOL JSM-6060) and high-resolution transmission electron microscopy (TEM, JEOL JEM-2010). The carbon contents of the nickel sulfide—carbon composite powders were measured from the energy dispersive spectroscopy (EDS) spectra. The Brunauer—Emmett—Teller (BET) surface

areas of the powders were measured using nitrogen gas as the adsorbate. The thermal behaviors of the bare nickel sulfide and nickel sulfide—carbon composite were studied by thermal gravimetric analysis (TGA, SDTA851) and differential scanning calorimeter (DSC, DSC823). The samples were heated at the heating rate of 10 °C min^{-1} in the temperature range of 30—900 °C.

The capacities and cycle properties of the bare nickel sulfide and nickel sulfide—carbon composites were measured using 2032-type coin cells. The electrodes were prepared using a slurry consisting of 70 wt% active anode material, 20 wt% carbon black (Super-P) as a conductive material, and 10 wt% binder composed of sodium carboxymethyl cellulose (CMC) on copper foil. Lithium metal and a microporous polypropylene film were used as the counter electrode and separator, respectively. Lithium hexafluorophosphate (1 M) in a mixture of ethylene carbonate (EC) and dimethyl carbonate (DMC) in a 1:1 volume ratio with 2 wt% vinylene carbonate (VC) was used as the electrolyte. The entire cell was assembled under an argon atmosphere in a glove box. The charge/discharge characteristics of the samples were measured at various current densities in the voltage range 0.01—3.0 V. Cyclic voltammetry measurements were carried out at a scan rate of 0.1 mV s^{-1} between 0.01 and 3 V. Electrochemical impedance spectra of the bare nickel sulfide and nickel sulfide—carbon composite were analyzed in the frequency range between 100 kHz and 10 MHz at room temperature with a signal amplitude of 5 mV.

3. Results and discussion

The crystal structures of the bare nickel sulfide and nickel sulfide—carbon composite powders prepared by spray pyrolysis are shown in Fig. 1. The nickel sulfide powders prepared without sucrose had mixed crystal structures consisting of NiS, Ni_7S_6, and Ni_xS_6 phases. The peak intensities of the NiS phase can be seen to decrease with increasing concentration of sucrose dissolved in the spray solution. The nickel sulfide—carbon composite powders prepared from the spray solution with 0.3 M sucrose had a pure crystal structure of Ni_7S_6 phase. A small peak corresponding to Ni_xS_6 [JCPDS card no. 00-051-0718] can be observed in the XRD pattern of the composite powders prepared with 0.1 M sucrose. No peaks resulting from nickel oxide are evident in the XRD patterns of the powders, irrespective of the concentration of sucrose used, demonstrating that the bare nickel sulfide and nickel sulfide—carbon composite powders were successfully prepared even with only an 8 s residence time inside the hot-wall reactor. The nickel sulfide—carbon composite powders prepared from the spray
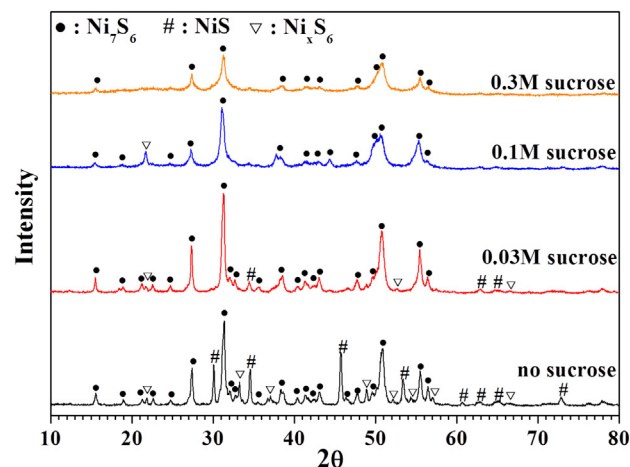

Fig. 1. XRD patterns of the bare nickel sulfide and nickel sulfide—carbon composite powders prepared by spray pyrolysis.

solutions with concentrations of sucrose above 0.1 M gave low peak intensities and broad peak widths because the high amount of carbon material disturbed the growth of the nickel sulfide crystals.

The morphology of bare nickel sulfide powders is shown in Fig. 2. The particles can be seen to have a spherical polygonal shape with some aggregation visible. The low and high-resolution TEM images in Fig. 2 show evidence of phase separation. The spherical polygonal powders can be seen to be connected, forming an amorphous material, as demonstrated by the arrows in Fig. 2. The dot-mapping images show that this amorphous material was sulfur-rich nickel sulfide. The melting and crystallization processes of the bare nickel sulfide powders inside the hot-wall reactor would be responsible for the phase-separated composite particles with several crystal phases. Different melting and crystallization characteristics of the different phases of nickel sulfides therefore resulted in the phase-separated material. Sulfur-rich nickel sulfide with a low melting temperature would move to the outer surface during the crystallization process at a high preparation temperature of 800 °C. A core–shell-like powder would first be formed as an intermediate product, and then, segregation of the sulfur-rich nickel sulfide would produce the Janus-like structured composite powder shown in the dot-mapping images. The merging of the nickel sulfide particles into one another was due to the melting of the sulfur-rich material.

The morphologies of the nickel sulfide–carbon composite powders prepared from a spray solution with 0.1 M sucrose are shown in Fig. 3. The composite particles can be seen to have a completely spherical shape, with no aggregation evident. The TEM and dot-mapping images and EDX line scans show a core–shell structure, as indicated by the dotted circles. The inner part of the particles was found to be rich in nickel and sulfide components, as shown by the dark areas in the TEM images. Segregation of nickel sulfide to the inner part of the composite particles occurred, resulting in the core–shell structure. The high-resolution TEM image of the composite powder shown in Fig. 3c demonstrates a mixed structure of crystalline nickel sulfide and amorphous carbon. Nickel sulfide crystals with a size of a few nanometers can be seen to be uniformly distributed throughout the amorphous carbon matrix. The high-resolution TEM image in Fig. 3c shows lattice fringes separated by 0.56 nm, which corresponds to the (002) plane of the cubic Ni_7S_6 phase. The selected area electron diffraction (SAED) pattern in Fig. 3c also shows that Ni_7S_6 crystals were formed by spray pyrolysis process.

The morphologies of the nickel sulfide–carbon composite powders prepared from the spray solutions with 0.03 and 0.3 M sucrose are shown in Figs. 4 and 5. The composite powders prepared with a concentration of sucrose as low as 0.03 M had completely spherical or polygonal shapes, as shown in the low resolution TEM image. Some rod-like crystals can also be seen in the high resolution TEM image in Fig. 4c. The carbon component was scarcely detected in the dot-mapping of the composite powders, as shown in Fig. 4d. When the sucrose concentration was as high as 0.3 M, the nickel sulfide–carbon composite particles had a spherical shape with a well facetted large crystal structure (Fig. 5). The dot-mapping images of the composite powders shown in Fig. 5d reveal that the well facetted crystals located on the outer
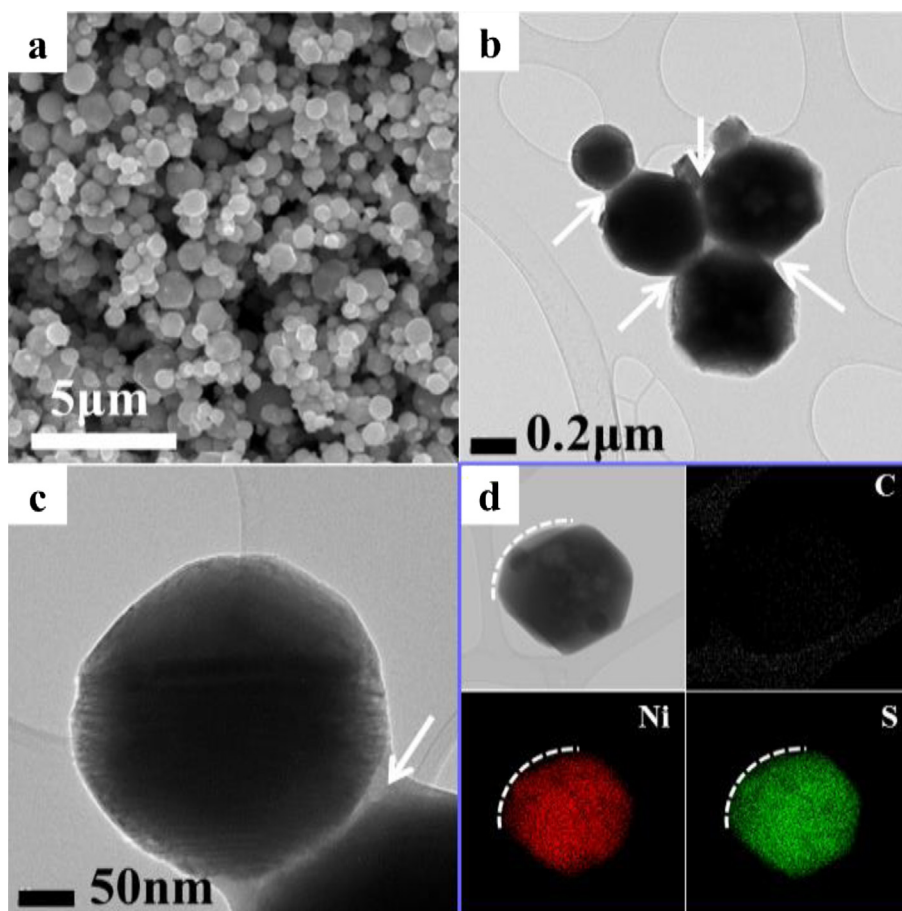

Fig. 2. Morphologies and dot-mapping images of the bare nickel sulfide powders prepared by spray pyrolysis.
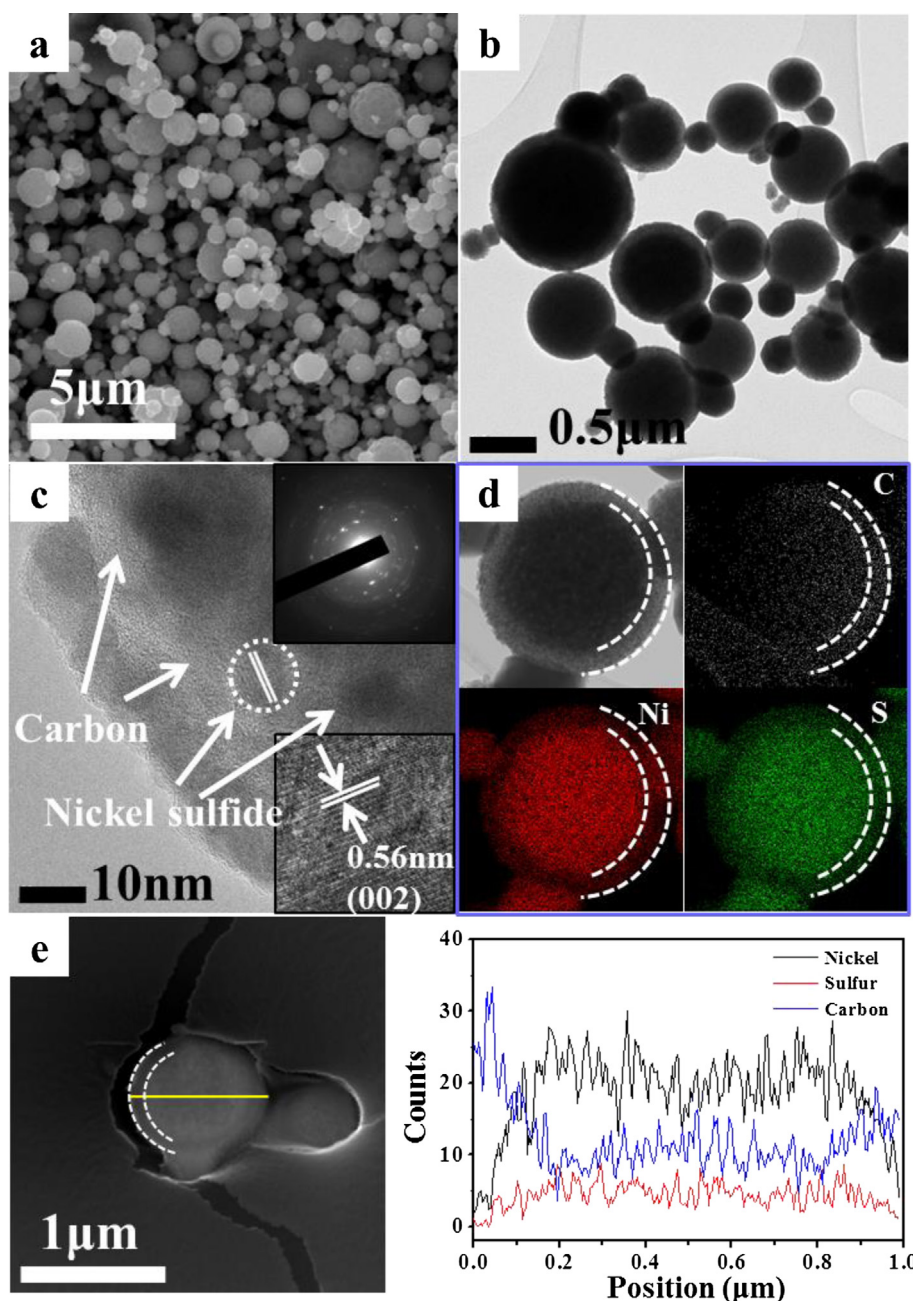
Fig. 3. Morphologies, dot-mapping images, and EDX line scan of the nickel sulfide–carbon composite powders prepared from the spray solution with 0.1 M sucrose.

surface were nickel sulfide. In contrast, the nickel sulfide located in the inner part of the particles had smaller crystals with a size of only a few nanometers, as shown in the high-resolution TEM image in Fig. 5c.

Fig. S1 shows the TG curves of the bare nickel sulfide and nickel sulfide–carbon composite powders prepared from the spray solutions without and with 0.1 M sucrose. TG analysis of the bare nickel sulfide powders showed a three-step weight loss and a two-step weight increase up to 900 °C. The first weight loss below 330 °C was associated with the loss of water adsorbed on the powders and partial decomposition of nickel sulfide. The abrupt weight loss above 640 °C was related to the decomposition of $NiSO_4$ intermediate into NiO. TG analysis of the nickel sulfide–carbon composite powders indicated a two-step weight loss up to 900 °C. The abrupt weight loss below 500 °C was associated with the decomposition of

carbon component in the composite powders. The weight increase due to formation of $NiSO_4$ offsets the weight decrease due to decomposition of carbon below 500 °C. The weight loss above 640 °C by decomposition of $NiSO_4$ intermediate into NiO was 8.1 wt % in the TG analysis of the nickel sulfide–carbon composite powders. The carbon contents of the powders prepared from the spray solutions with 0.03, 0.1, and 0.3 M sucrose measured from the EDS spectra as shown in Fig. S2 were 3, 17, and 24 wt%, respectively.

The mechanisms by which the bare nickel sulfide and nickel sulfide–carbon composite powders were formed are shown in Scheme 1, according to the concentrations of sucrose dissolved in the spray solutions. In the front part of the reactor, nickel oxide powders were first formed by drying and deconstruction of the droplets. Fast decomposition of thiourea at high temperatures then resulted in the evolution of hydrogen sulfide gas, forming a
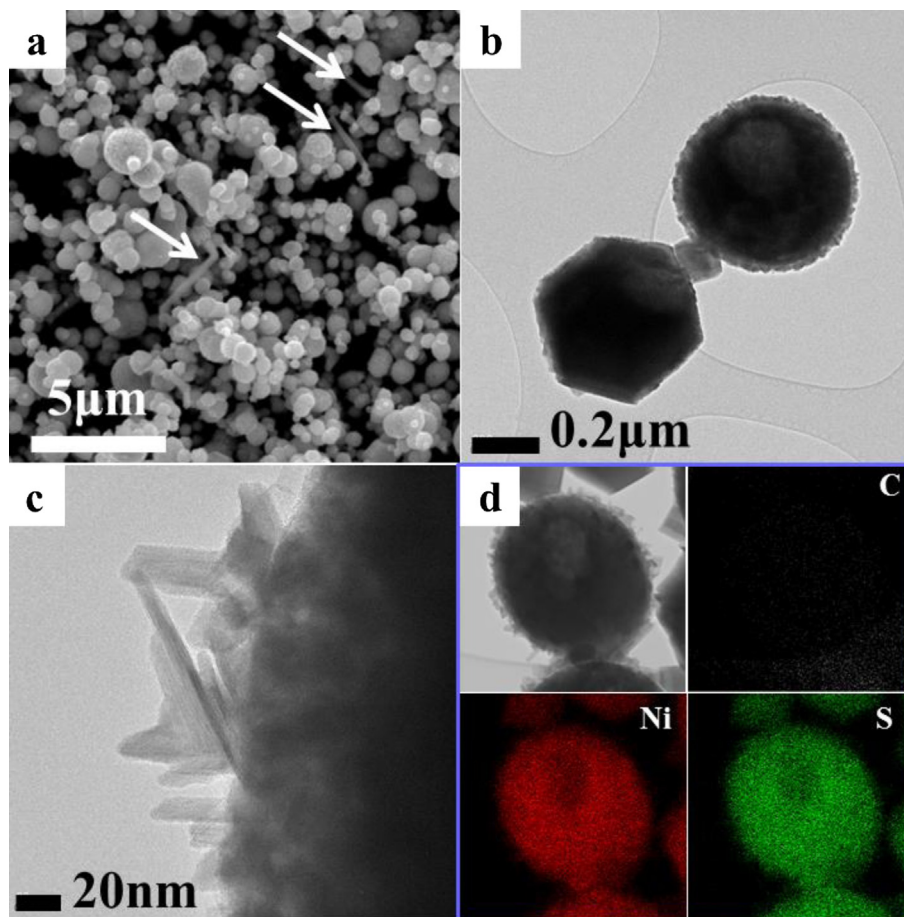
Fig. 4. Morphologies and dot-mapping images of the nickel sulfide–carbon composite powders prepared from the spray solution with 0.03 M sucrose.

reducing atmosphere inside the reactor. The polymerization and carbonization of sucrose produced nickel oxide–carbon composite powders as an intermediate product. Sulfidation of NiO by hydrogen sulfide gas occurred *via* a two-step process to generate the nickel sulfide–carbon composite powders in the rear part of the reactor. Ni metal was generated by reduction of NiO under the reducing atmosphere. Immediate reaction of hydrogen sulfide gas with Ni metal generated nickel sulfide. Crystal growth of the nickel sulfide was minimized by the carbon matrix; therefore, nickel sulfide nanocrystals that were a few nanometers in size were uniformly distributed inside the spherical carbon matrix when the concentration of sucrose was 0.1 M. The high content of carbon in the nickel sulfide–carbon composite powders prepared from the spray solution containing 0.3 M sucrose increased the reducing power of the atmosphere around the composite particles. Therefore, large crystals of nickel metal were formed at the surface of the composite particles by reduction of nickel oxide. The subsequent sulfidation of the nickel metal produced large Ni_7S_6 crystals around the surface of the Ni_7S_6–carbon composite powders. Therefore, it was deduced that the optimum concentration of sucrose for preparing nickel sulfide–carbon composite powders with a uniform structure was 0.1 M.

The measured electrochemical properties of bare nickel sulfide and the nickel sulfide–carbon composite powders are shown in Fig. 6. The initial charge and discharge curves of the nickel sulfide composite powders prepared with different concentrations of sucrose at a constant current density of 1000 mA g^{-1} are shown in Fig. 6a. Similar initial charge and discharge curves can be observed,

irrespective of the sucrose concentration, even though they were demonstrated to have different crystal structures. The plateaus around 1 V in the initial discharge curves could be as a result of nickel reduction, and the plateaus at approximately 2 V in the initial charge could be due to generation of Ni_xS_y [21,22]. The cyclic voltammograms of the bare nickel sulfide and nickel sulfide–carbon composite powders were shown in Fig. S3. The potential scan rate was 0.1 mV s^{-1}, with the voltage raging between 0.01 and 3 V. In the initial discharge cycle, strong and weak cathodic peaks were observed at around 1 and 1.6 V, respectively, irrespective of carbon contents of the composite powders. The weak cathodic peak was attributed to the transformation of NiS to Ni_3S_2. Also, the strong cathodic peak was due to the reduction of Ni_3S_2 and Ni_7S_6 to Ni, the formation of amorphous Li_2S, and a solid electrolyte interphase (SEI) layer. In subsequent cycles, the strong cathodic peak shifted to higher voltage ranges. The strong anodic peak at around 2.1 V could be associated with the oxidation of metallic Ni [9,15,22–24]. The initial discharge capacities and Coulombic efficiencies of the nickel sulfide powders were strongly affected by the carbon content. The bare nickel sulfide powders had initial discharge and charge capacities of 802 and 475 mA h g^{-1}, respectively, and the corresponding initial Coulombic efficiency was as low as 59%. The structural breakdown of bare nickel sulfide powder with submicron particles and a dense structure during the first cycle decreased the initial Coulombic efficiency. The nickel sulfide powders prepared from the spray solution with 0.03 M sucrose had high initial discharge and charge capacities of 950 and 733 mA h g^{-1}, respectively, and the corresponding initial Coulombic efficiency was as
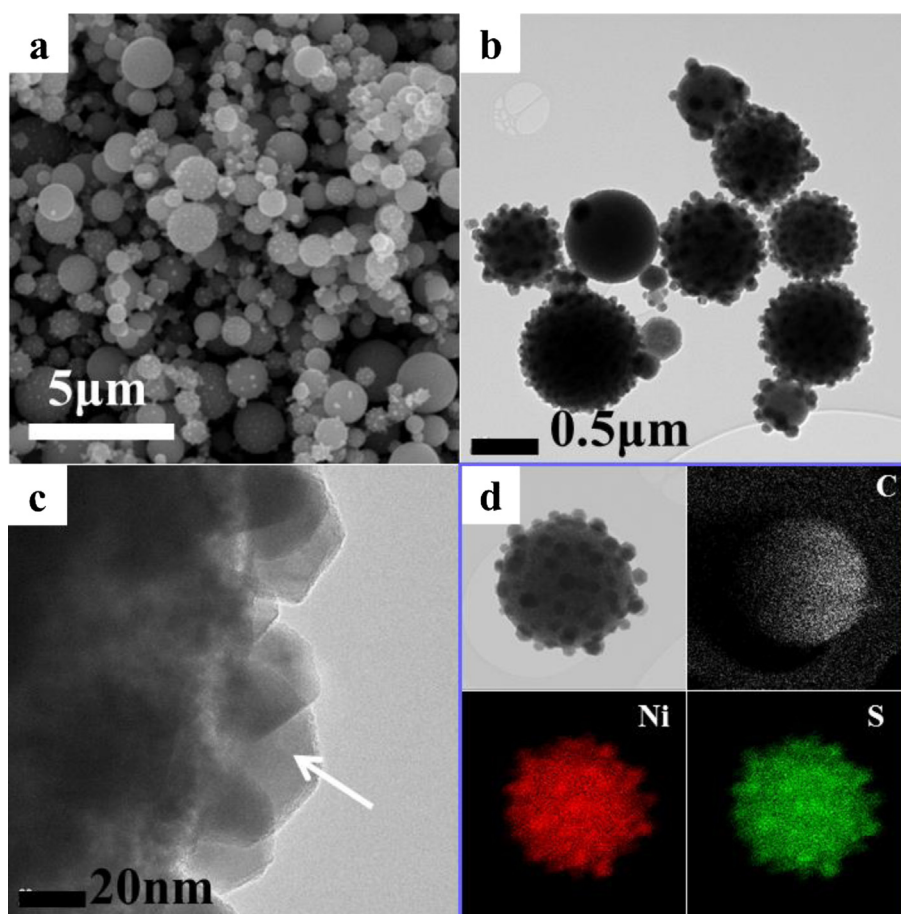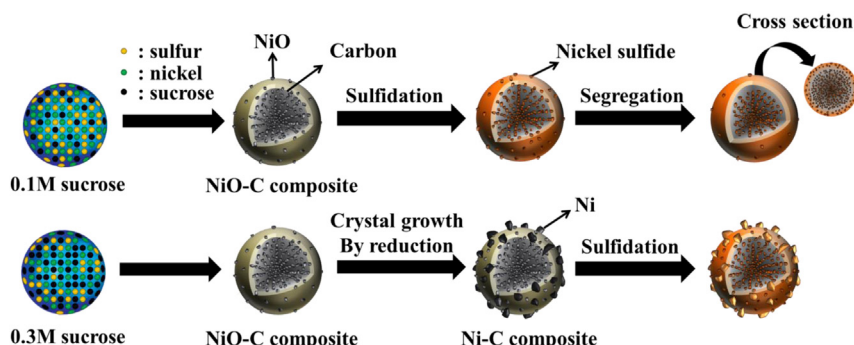
Fig. 5. Morphologies and dot-mapping images of the nickel sulfide–carbon composite powders prepared from the spray solution with 0.3 M sucrose.

high as 77%. On the other hand, nickel sulfide–carbon composite powders prepared with 0.1 and 0.3 M sucrose had lower initial Coulombic efficiencies of 63 and 56%, respectively. A high amount of amorphous carbon clearly lowered the initial Coulombic efficiencies of the composite powders prepared with high concentrations of sucrose in the spray solutions. Fig. 6b shows the long cycling performances of the nickel sulfide powders at a constant current density of 1000 mA g^{-1}. The bare nickel sulfide powders showed extremely fast capacity fading characteristics, with discharge capacities of 453, 117, and 65 mA h g^{-1} in the 2nd, 100th, and 200th cycles, respectively. The discharge capacities of the nickel sulfide composite powders prepared with 0.03 M sucrose slowly decreased from 950 to 540 mA h g^{-1} during the first 100

cycles, and then sharply decreased to 25 mA h g^{-1} during the following 100 cycles. However, the nickel sulfide–carbon composite powders prepared with higher sucrose concentrations of 0.1 and 0.3 M retained high discharge capacities, with values of 472 and 273 mA h g^{-1} exhibited after 500 cycles, respectively, corresponding to capacity retentions after the first cycles of 86 and 50%, respectively. The large size of the nickel sulfide crystals appeared to decrease the cycling performance of the composite powders prepared from the spray solution with 0.3 M sucrose. The optimum amount of carbon component for high discharge capacities and good cycling performance was therefore identified to be formed from the spray solution containing 0.1 M sucrose. The rate performance of the nickel sulfide–carbon composite powders prepared

Scheme 1. Mechanisms of formation of the nickel sulfide–carbon composite powders in the spray pyrolysis system.
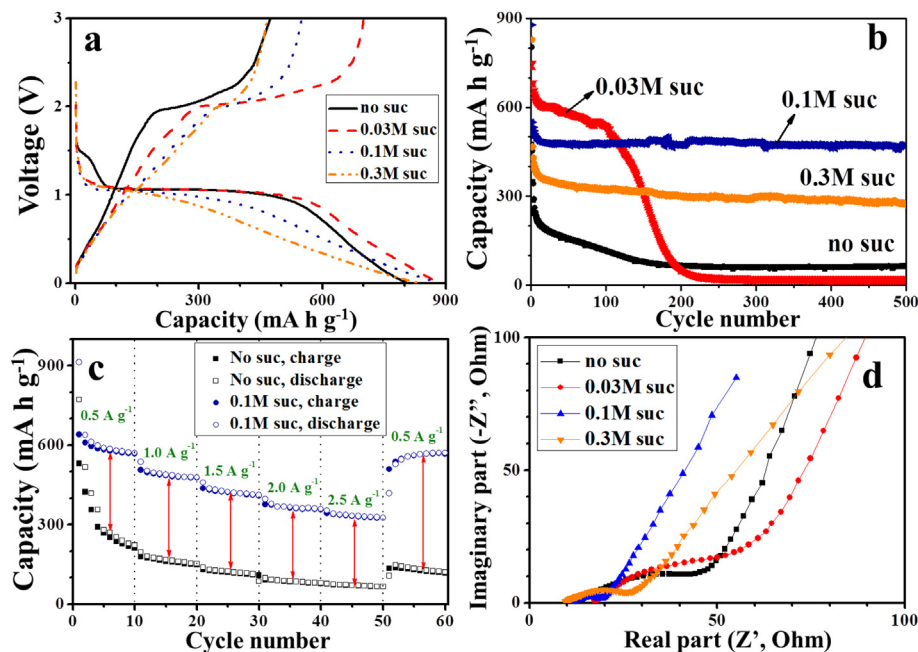
Fig. 6. Electrochemical properties of the bare nickel sulfide and nickel sulfide–carbon composites powders prepared by spray pyrolysis with various concentrations of sucrose; (a) initial charge and discharge curves, (b) cycling performances, (c) rate performances, (d) Nyquist impedance plots.
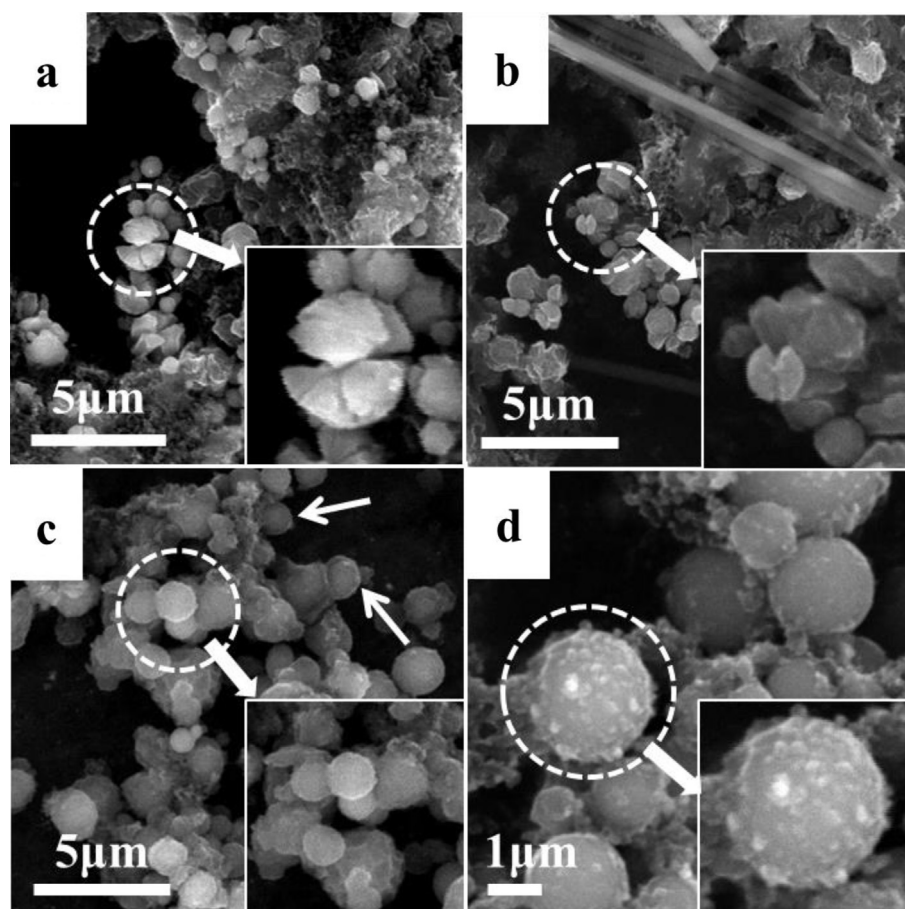

Fig. 7. Morphological changes of the powders after 500 cycles; (a) no sucrose, (b) 0.03 M sucrose, (c) 0.1 M sucrose, (d) 0.3 M sucrose.

with 0.1 M sucrose are shown in Fig. 6c, where the current densities were increased stepwise from 500 to 2500 mA g^{-1} in the voltage range of 0.01–3. V. For each step, 10 cycles were measured to evaluate the rate performance. The composite powders exhibited final cycle capacities of 571, 479, 412, 358, and 327 mA h g^{-1} at current densities of 500, 1000, 1500, 2000, and 2500 mA g^{-1}, respectively. To further study the effect of the carbon component, Nyquist impedance plots obtained after 500 cycles were obtained (Fig. 6d). The semicircle diameters in the medium-frequency region for the bare nickel sulfide and nickel sulfide–carbon composite with low carbon content can be observed to be larger than those of the composites with high carbon contents. The values of charge-transfer resistance (R_{ct}) for the powders prepared from the spray solutions with 0, 0.03, 0.1, and 0.3 M sucrose are 27, 33, 8, and 16 Ω, respectively. The structural stability of the nickel sulfide–carbon composite powders prepared from the spray solution with 0.1 M sucrose appeared to minimize the charge-transfer resistance during cycling at high current densities. Fig. 7 shows the morphological changes that occurred for all of the different powders after 500 cycles. The bare nickel sulfide and nickel sulfide–carbon composite powders (Fig. 7a and b) with low carbon content can be seen to have a non-spherical shape after cycling, and the initial submicron-sized spherical particles appear to have been broken into several pieces. On the other hand, the nickel sulfide–carbon composite powders (Fig. 7c and d) with high carbon content maintained their spherical shapes even after 500 cycles at a high current density of 1000 mA g^{-1}. The carbon component appeared to effectively buffer the large volume changes of the nickel sulfide electrodes during the repeated charging and discharging [25].

4. Conclusions

The electrochemical properties of nickel sulfide–carbon composite powders were compared to those of the bare nickel sulfide powders prepared using the same spray pyrolysis process. The concentration of the sucrose used as the carbon source in the spray solution affected the crystal structures and morphologies of the nickel sulfide powders. It was found that the optimum concentration of sucrose for preparing a nickel sulfide–carbon composite powder with uniform composition and good electrochemical properties at high current densities was 0.1 M. The produced carbon matrix appeared to act as a buffer layer to cushion the effects of the severe volume expansion that occurred during the repeated charge and discharge cycling. The powders prepared using 0.1 M sucrose could endure the volume changes without significant loss of discharge capacity up to 500 cycles. The nickel sulfide–carbon composite powders prepared by spray pyrolysis had a high initial discharge capacity, high capacity retention, and good rate performances, in contrast to the poor cycling ability of the bare nickel sulfide material.

Appendix A. Supplementary data

Supplementary data related to this article can be found at http://dx.doi.org/10.1016/j.jpowsour.2013.10.093.

References

[1] C.-H. Lai, M.-Y. Lu, L.-J. Chen, J. Mater. Chem. 22 (2012) 19.
[2] B. Zhang, X.C. Ye, W. Dai, W.Y. Hou, Y. Xie, Chem. Eur. J. 12 (2006) 2337.
[3] A. Manthiram, Y.U. Jeong, J. Solid State Chem. 147 (1999) 679.
[4] H.T. Zhang, G. Wu, X.H. Chen, Mater. Lett. 59 (2005) 3728.
[5] Y. Wang, Q. Zhou, L. Tao, X. Su, J. Mater. Chem. 21 (2011) 9248.
[6] A. Ghezelbash, B.A. Korgel, Langmuir 21 (2005) 9451.
[7] K. Aso, H. Kitaura, A. Hayashi, M. Tatsumisago, J. Mater. Chem. 21 (2011) 2987.
[8] Z.-S. Wu, W. Ren, L. Wen, L. Gao, J. Zhao, Z. Chen, G. Zhou, F. Li, H.-M. Chen, ACS Nano 4 (2010) 3386.
[9] J.-Z. Wang, S.-L. Chou, S.-Y. Chew, J.-Z. Sun, M. Forsyth, D.R. MacFarlane, H.-K. Liu, Solid State Ionics 179 (2008) 2379.
[10] X.J. Liu, Z.Z. Xu, H.J. Ahn, S.K. Lyu, I.S. Ahn, Powder Technol. 229 (2012) 24.
[11] T. Takeuchi, H. Sakaebe, H. Kageyama, K. Handa, T. Sakai, K. Tatsumi, J. Electrochem. Soc. 156 (2009) A958.
[12] N. Mahmood, C. Zhang, Y. Hou, Small 9 (2013) 1321.
[13] L. Zhou, Y. Wu, L. Wang, Y. Yu, X. Zhang, F. Zhao, RSC Adv. 2 (2012) 5084.
[14] C. Zhang, R. Hao, H. Yin, F. Liu, Y. Hou, Nanoscale 4 (2012) 7326.
[15] S. Ni, X. Yang, T. Li, Mater. Chem. Phys. 132 (2012) 1103.
[16] S.E. Skrabalak, K.S. Suslick, J. Am. Chem. Soc. 127 (2005) 9990.
[17] K. Okuyama, I.W. Lenggoro, N. Tagami, J. Mater. Sci. 32 (1997) 1229.
[18] I.W. Lenggoro, K. Okuyama, J.F. de la Mora, N. Tohge, J. Aerosol Sci. 31 (2000) 121.
[19] J.H. Bang, R.J. Helmich, K.S. Suslick, Adv. Mater. 20 (2008) 2599.
[20] S. Liu, H.W. Zhang, M.T. Swihart, Nanotechnology 20 (2009) 235603.
[21] T. Matsumura, K. Nakano, R. Kanno, A. Hirano, N. Imanishi, Y. Takeda, J. Power Sources 174 (2007) 632.
[22] N.H. Idris, M.M. Rahman, S.L. Chou, J.Z. Wang, D. Wexler, H.K. Liu, Electrochim. Acta 58 (2011) 456.
[23] H.Q. Dai, Y.N. Zhou, Q. Sun, F. Lu, Z.W. Fu, Electrochim. Acta 76 (2012) 145.
[24] N. Feng, D. Hu, P. Wang, X. Sun, X. Li, D. He, Phys. Chem. Chem. Phys. 15 (2013) 9924.
[25] Y. Li, J.P. Tu, X.H. Huang, H.M. Wu, Y.F. Yuan, Electrochem. Commun. 9 (2007) 49.